ELSEVIER

Chemical Physics 201 (1995) 141–150

Chemical Physics

# Size quantization and surface states of molybdenum sulphide clusters: a molecular orbital approach

Martin Brändle, Gion Calzaferri *, Martin Lanz

*Institute for Inorganic, Analytical and Physical Chemistry, University of Bern, Freiestrasse 3, CH-3012 Bern, Switzerland*

Received 8 June 1995

**Abstract**

A projection procedure is described, as a tool to separately analyze the electronic states of surface and bulk regions of nanometer-sized particles. It allows to discuss surface states in terms of specific atoms, coordination numbers, oxidation states, and connectivities and it gives insight into the size quantization of clusters. The procedure is general and can be used for studying clusters up to respectable size, of different composition and different structure. Molecular orbital calculations on $D_{3h}-(MoS_2)_{3n^2}S_2(H_2S)_{6n}$, $n=1,2,\cdots$ clusters, cluster chains and the band structure of $^2_\infty[MoS_2]$ are reported. The HOMO and LUMO are separated by only about 0.1 eV in $Mo_{12}S_{38}H_{24}$. Even this small splitting vanishes in the larger clusters. However, in the limiting infinite case, $^2_\infty[MoS_2]$, the expected semiconductor band gap evolves. Applying the projection procedure to the clusters we find that surface states, originating from the outermost molybdenum atoms and being of mainly $4d_{x^2-y^2}$, $4d_{xy}$, and $4d_{z^2}$ type with some S(3p) contributions, fill up the band gap and that the bulk shows the expected quantum-size behaviour.

## 1. Introduction

The discussion of *surface states* has continued since the memorable 1932 paper of I. Tamm in which he created this expression [1]. Tamm considered the wave functions for an idealized semi-infinite, one-dimensional crystal in which the atomic fields were represented by square potential wells. He found that it is possible to have energy levels the wave functions of which are localized at the surface of the crystal and that one surface level is possible for each energy gap between the ordinary allowed bands of energies. The theoretical studies on surface states were continued by Goodwin [2], Shockley [3], Koutecky [4], Hoffmann [5], and others. On the other side the special properties of small particles have occupied the minds of chemists for nearly a century now [6]. However, the understanding of the *quantum-size effect*, for which the dramatic colour change of CdS particles as a function of their size is an example [7], has been advanced by the theoretical work of Brus published in 1983 [8]. He presented a simple model for the ionization potential, the electron affinity and the aqueous redox potential of small semiconductor crystallites. The eigenvalue solutions of the particle in a box motion were combined with an electrostatic potential for dielectric polarization inside a charged sphere. The model describes the

* Corresponding author.


*SSDI* 0301-0104(95)00272-3

behaviour of "bulk" states in the limit of small crystallites. Finite depth well potentials were discussed later by Rajh et al. [9], by Nosaka [10], and others.

The surface states as described in the early studies and the particle in a spherical box model of Brus are based on general quantum mechanical considerations. They do not convey straightforward chemical information, which means assignment of the resulting states to specific atoms, molecules, coordination numbers, oxidation states, and connectivities. Messmer and Watkins published an EHMO (extended Hückel molecular orbitals) study on the vacancy in diamond already in 1971 [11], and a theoretical approach to surface structure and reactivity that is within the framework of solid-state theory, yet strives for chemical ways of interpretation, was developed by Hoffmann [5]. In this successful way to look at bonding on surfaces one begins at highly delocalized band structures. Interpretational tools – density-of-states decompositions and crystal orbital overlap populations – allow a tracing of local, chemical acts [12]. The reciprocal space approach to the orbitals of truncated crystals as described by Hoffmann et al. is another top-down approach to derive the orbitals of large finite systems such as clusters from crystal orbitals of a solid [13]. On the other hand EHMO calculations on clusters of remarkable size have recently become relatively easy and inexpensive [14,15] and the question arises how and to what extent such calculations can help to improve our understanding of nanometer-sized particles. Interpretational tools to decompose surface states from the bulk states are needed because of the large number of states of such particles. In this report we focus on a projection procedure of the molecular orbitals of clusters based on Mulliken population analysis as an instrument to analyze the electronic states of surface and bulk contributions separately. Clusters of layered materials with equivalent top and bottom surface atoms are easier to be described than other structures because only the periphery atoms have to be considered apart, and they have been chosen in the present report for this reason.

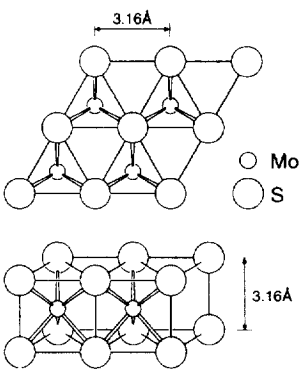


Scheme 1. $MoS_2$ layer structure with trigonal prismatic coordination of the Mo.

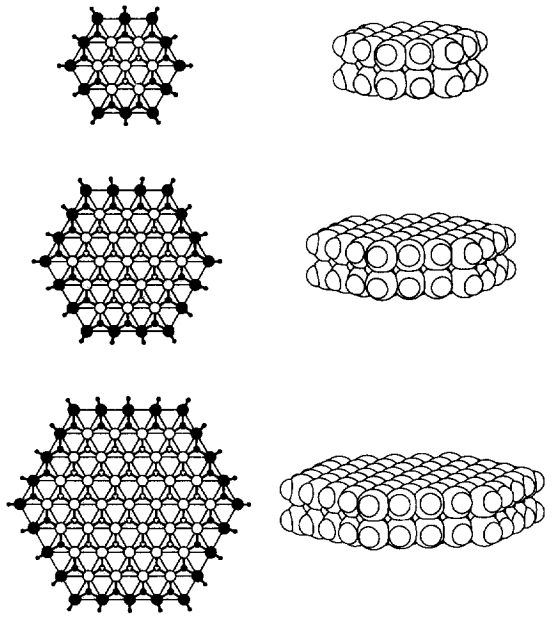

Scheme 2. $D_{3h}-(MoS_2)_{3n^2}S_2(H_2S)_{6n}$ clusters. Clusters with $n = 2$, 3, and 4 are shown. Atoms assigned to the surface shell are shaded.

Many transition-metal dichalcogenides display a characteristic layered structure [16]. Two-dimensional slabs are formed by two layers of close-packed chalcogenide atoms sandwiching one metal layer between them in $MX_2$ (X = S,Se). Then these $MX_2$ slabs are stacked, with just van der Waals contacts between them. The two chalcogenide layers forming a slab can be stacked directly above each other, making trigonal prismatic holes for the metals. This is shown in Schemes 1 and 2 for $MoS_2$. Alternatively, the layers may stagger forming octahedral

holes. The general features of the energy bands of these two structures have been discussed [17]. These layered materials have demonstrated respectable sunlight to electrical energy conversion efficiencies and remarkable stability to photocorrosion when employed in photoelectrochemical cells [18,19]. They are catalysts [20] and they show interesting intercalation properties [21]. In this study we focus on the trigonal prismatic structure and we discuss $MoS_2$, for which the formation of quantized colloids by simple dissolution of crystalline powder in acetonitrile has been reported [22]. An ideal stoichiometric $MoS_2$ layer can terminate with 6-fold, 4-fold and 2-fold $Mo^{4+}$ coordinations to $S^{2-}$ [23]. Out of them, the 6-fold coordination is the only one in which the "inner" Mo atoms have the same coordination shell as the "outer" ones. This means that it is the idealest and therefore simplest case to be studied. Coordination of the free valence of the outer S atoms with H serves to saturate the dangling bonds. It simplifies the calculations and the discussion but does not affect the states dealt with here. This leads to the $D_{3h}$ – $(MoS_2)_{3n^2}S_2(H_2S)_{6n}$, $n = 1,2, \cdots$ clusters illustrated in Scheme 2. These particles do not display size quantization. However, applying the projection procedure, we will show that their one-electron states can be divided into bulk- and shell-localized states, and that the bulk shows the expected quantum-size behaviour [24].

## 2. Computational procedure

*Structure.* The structure of a $^2_\infty[MoS_2]$ layer as determined by Dickinson and Pauling already in 1923 is shown in Scheme 1 [25]. The distance between two sulphur atoms within and across the chalcogenide plane is about 3.16 Å. The clusters in Scheme 2 are based on this structure with constant Mo–S bond distances of 2.41 Å. The free valence of the outermost sulphur atoms is saturated with hydrogen, the 1.33 Å hydrogen–sulphur bonds pointing to the cluster center. Thus the symmetry is $D_{3h}$ and the stoichiometry can be expressed as $(MoS_2)_{3n^2}S_2(H_2S)_{6n}$, $n = 1,2, \cdots$, where $n$ denotes the number of molybdenum shells. We report calculations on clusters with $n$ up to 4. Table 1 shows how they grow with increasing $n$. It also contains the number of valence atom orbitals (AOs) that form the basis for the molecular orbital (MO) and the band structure calculations.

Table 2
Coulomb integrals $H_{ii}$ (eV) and Slater exponents $\zeta_i$

| Element | Orbital | $\zeta_i$ ($c_i$) | $H_{ii}$ (eV) |
|---|---|---|---|
| Mo | 5s | 1.96 [27] | −8.94 |
| | 5p | 1.90 [27] | −5.60 |
| | $4d_1$ | 3.814 (0.512) [28] | −10.43 |
| | $4d_2$ | 1.864 (0.641) [28] | |
| S | 3s | 2.283 [29] | −19.85 |
| | 3p | 1.817 [29] | −10.93 |
| H | 1s | 1.3 | −13.6 |

*MO calculations.* MO calculations have been carried out by the extended Hückel method [26], with the parameters listed in Table 2. The off-diagonal elements were calculated as [30]

$$H_{ij} = \tfrac{1}{2}kS_{ij}(H_{ii} + H_{jj}) \quad (1)$$

by using the weighted Wolfsberg–Helmholz formula [31] with a distance-dependent Hückel constant [14,32] and the parameters $\kappa = 0.64$, $\delta = 0.35$ Å$^{-1}$. The Coulomb integrals $H_{ii}$ for the molybdenum and the sulphur atoms were obtained by charge iteration on the cluster $Mo_{48}S_{122}H_{48}$ with the parameters from Refs. [33,34].

Table 1
Properties of the clusters shown in Scheme 2

| Cluster | Bulk | Surface | Total number of valence AOs | Number of bulk valence AOs | Number of surface valence AOs | Cluster diameter (nm) |
|---|---|---|---|---|---|---|
| $Mo_{12}S_{38}H_{24}$ | $Mo_3S_{14}$ | $Mo_9S_{24}H_{24}$ | 284 | 83 | 201 | 1.6 |
| $Mo_{27}S_{74}H_{36}$ | $Mo_{12}S_{38}$ | $Mo_{15}S_{36}H_{36}$ | 575 | 260 | 315 | 2.2 |
| $Mo_{48}S_{122}H_{48}$ | $Mo_{27}S_{74}$ | $Mo_{21}S_{48}H_{48}$ | 968 | 539 | 429 | 2.9 |

*Projection.* As an initial guess, clusters were separated on an intuitive basis into a part belonging to the bulk and a part described as shell. The so defined bulk and shell formed the fragments for an LCFMO [14,35] (linear combination of fragment molecular orbitals) calculation. The initial guess was then refined based on the criterion that the bulk part should be made as large as possible and the shell as thin as possible. According to Mulliken population analysis [36] the charge contribution $Q_{iR_k}$ of the fragment MO $R_k$ to the cluster MO $i$ is given by

$$Q_{iR_k} = 2c_{iR_k}\left(c_{iR_k} + \sum_{S_l \neq R_k} c_{iS_l} S_{R_k S_l}\right), \tag{2}$$

$c_{iR_k}$ and $c_{iS_l}$ are the FMO coefficients of the fragment MOs $R_k$ and $S_l$ on the fragments $R$ and $S$, respectively. $S_{R_k S_l}$ is the overlap integral between the fragment MOs $R_k$ and $S_l$. The first contribution is the charge density coming from the fragment $R$. The second contribution is half of the charge density between the fragments $R$ and $S$, which is an indicator for the interaction between them. The charge contributions of the bulk and of the shell are the sum over all bulk and over all shell FMO contributions, respectively:

$$Q_i(\text{bulk}) = \sum_{R_k \in \text{bulk}} Q_{iR_k}, \tag{3}$$

$$Q_i(\text{shell}) = \sum_{R_k \in \text{shell}} Q_{iR_k}.$$

The sum of the bulk and the shell charge contributions is 2, which is the total electron occupation of each orbital $i$.

$$Q_i(\text{bulk}) + Q_i(\text{shell}) = 2. \tag{4}$$

The charges $Q_i$(bulk) and $Q_i$(shell) served as sorting criterion for the classification of the levels into states where the wave function is mainly localized on the bulk and on the shell, respectively. If the charge contribution of the shell atoms was larger than the ratio of the number of shell atom AOs to the total number of cluster AOs, the cluster MO was attributed to the shell, otherwise to the bulk. This makes the criterion independent of the cluster size, which means that different clusters can be compared with each other. We will show that it is useful to plot the quantity $\Delta Q_i$ for each level $i$.

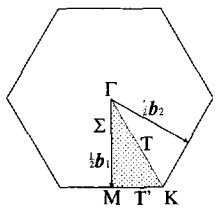


Scheme 3. Hexagonal Brillouin zone.

$$\Delta Q_i = Q_i(\text{shell}) - Q_i(\text{bulk}). \tag{5}$$

*Band structure calculations.* The cluster chain and the $^2_\infty[MoS_2]$ calculations were performed within the framework of the extended Hückel tight-binding method [37,38] in its ASED modification [39], with the same parameters as used for the MO investigations. For the infinite monolayer the hexagonal Brillouin zone shown in Scheme 3 was used. The density of states was obtained by fitting Gaussian lobes $N_j \exp[-(E_i - E_j)^2/\sigma^2]$ with half-width $\sigma$ to the energy level distribution, counting the levels $E_i$ centered around a mesh point $E_j$ within the range $E_j - 3\sigma \cdots E_j + 3\sigma$. A large half-width of the Gaussians therefore averages the DOS contributions over a bunch of levels, a very small half-width of about 1–2 meV allows to trace single levels.

*Cluster chains.* To apply the band structure program package [38] for the clusters in Scheme 2 one can stack them to form an infinite chain with translational symmetry perpendicular to their planes. The distance between the clusters can be chosen so large that cluster–cluster interactions become negligible. 10 Å was applied in our calculations. The translational symmetry allows to use the language of solid state physics, turning from MOs to crystal orbitals (COs) and from single energy levels to energy bands and the corresponding density of states (DOS). The information obtained is the same as in the MO calculations, only the language is slightly different. The properties were averaged over 6 equally distributed $k$-points in the first irreducible linear Brillouin zone. Since the crystal orbitals are expressed as linear combinations of Bloch sums over atomic orbitals, orbital contributions of a single atom or sev-

eral atoms can be projected out of the total DOS, which was done for the shell of the cluster chains. Assignment of the states to the shell and to the bulk was based on the ratio of the number of shell atom orbitals to the total number of cluster AOs as in the MO calculations. If in a given energy range the ratio of projected shell density to the total density of states was larger than this ratio, the total DOS was attributed to the shell, else to the bulk.

## 3. Results and discussion

Molybdenum sulphide is an indirect optical d–d band gap semiconductor [17,18,40]. This is well reflected in the band structure of an infinitely extended $^{2}_{\infty}[MoS_2]$ slab along the hexagonal Brillouin zone symmetry lines, Scheme 3, and in the DOS plot shown in Fig. 1. Stacking several of these layers with just van der Waals contacts between the slabs has only little influence on the results of our calculations. The position of the Fermi level and the trigonal prismatic coordination of the $Mo^{4+}$ is typical for a $d^2$ transition metal chalcogenide as was discussed by Hoffmann [17]. The top of the valence band is situated at Γ. The smallest direct transition is found at the point K of the Brillouin zone. From the DOS plot, where the S(3s), S(3p) and the Mo(4d) contributions have been projected out, it is evident that the lowest band is mainly composed of S(3s) derived states. At the top of the valence band is the so-called $d_{z^2}$ band. It overlaps slightly with the binding part of the valence band, which is predominantly of S(3p) character with mixed-in Mo(4d) contributions. The Fermi level is calculated to be at −9.87 eV. The smallest direct gap is situated at K and the smallest indirect gap goes from Γ to K, with values of 0.68 and 0.47 eV, respectively. The calculated charges are +0.30 on Mo and −0.15 on S. These results are in good agreement with the experimental data and also with more sophisticated calculations [40–42]. The calculated band gaps are too small, but they can be adjusted by optimizing the Slater orbital coefficients. We have not done this, but we have verified that the too small calculated band gap does not affect our conclusions.

The ideal infinitely extended $^{2}_{\infty}[MoS_2]$ is free of surface states. This means that no states are present within the energy gap between the valence and the conduction band. Another way to express this is to say that the van der Waals surface is saturated. We now consider the energy level diagrams of $Mo_{12}S_{38}H_{24}$, $Mo_{27}S_{74}H_{36}$ and $Mo_{48}S_{122}H_{48}$ in Fig. 2 and concentrate on the left rows for a moment. The

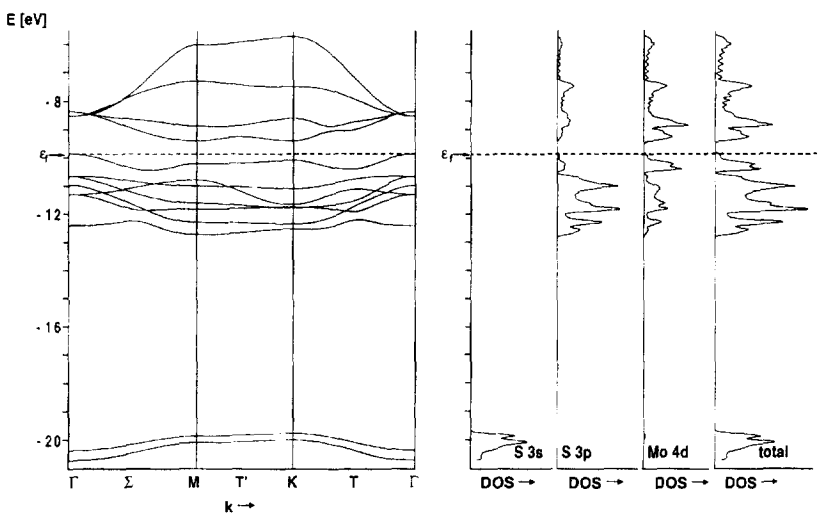


Fig. 1. Band structure along the hexagonal Brillouin zone symmetry lines and density of states of a $^{2}_{\infty}[MoS_2]$ layer. The S(3s), S(3p) and Mo(4d) contributions to the DOS are projected out.

number of one-electron states calculated equals the total number of valence AOs in Table 1. Comparison with Fig. 1 shows, that many surface states are present in these clusters. Which atoms of the clusters are responsible for the surface states? Applying the projection procedure as explained in the computational section to the cluster MOs leads to the result that the outermost Mo and S atoms, which are shaded in Scheme 2, are responsible for the surface states and thus form the shell, including the H atoms which only serve to saturate the dangling bonds. The shell is fundamentally different from the "saturated" van der Waals surface. Its stoichiometric formula is $Mo_{6n-3}S_{12n}H_{12n}$ and that of the unshaded bulk is $Mo_{3(n-1)^2}S_{6n^2-6n+2}$.

The smallest cluster $Mo_3S_{14}H_{12}$ of the $D_{3h}$ – $(MoS_2)_{3n^2}S_2(H_2S)_{6n}$, $n = 1,2,\cdots$ family is not shown in Fig. 2 because it consists only of surface atoms. On the left side of each of the three diagrams the positions of the cluster one-electron energy levels in the range from $-12$ to $-6$ eV are indicated by a bar. The position of the HOMO as obtained by applying the aufbau principle is marked by an arrow. For a growing cluster up to an infinite layer the HOMO becomes the $\Gamma$ point in Fig. 1, indicated as Fermi energy $\epsilon_f$, and the indirect band gap should become visible as HOMO/LUMO splitting of the cluster. For quantum-sized particles this HOMO/LUMO splitting is expected to be largest for the smallest clusters and to approach the limiting minimum value of $^2_\infty[MoS_2]$ with growing size. However, we observe that the HOMO and LUMO are separated by only about 0.1 eV in $Mo_{12}S_{38}H_{24}$ and that even this small splitting vanishes in the larger clusters. This means that they are paramagnetic without bearing any quantum-size character. In the limiting $^2_\infty[MoS_2]$ case, however, a band gap evolves, see Fig. 1. Applying the procedure as described in the computational section, Eqs. (2)–(5), the levels belonging to the bulk and to the shell can be projected out. This separates levels belonging to wave functions localized on the bulk from those localized on the shell. Fig. 3 explains how it works. On its right side we show the $\Delta Q_i$ charge, Eq. (5), for each energy level of the $Mo_{48}S_{122}H_{48}$ cluster from $-12$ to $-6$ eV. This difference is $-2$ if the wave function is completely localized on the bulk, it is zero if half of the charge is on the bulk and half on the shell and it is 2 if all charge is on the shell. As in any kind of projection there are instances for which the assignment is to some extent arbitrary. In the present case, however, the assignment of the levels of the

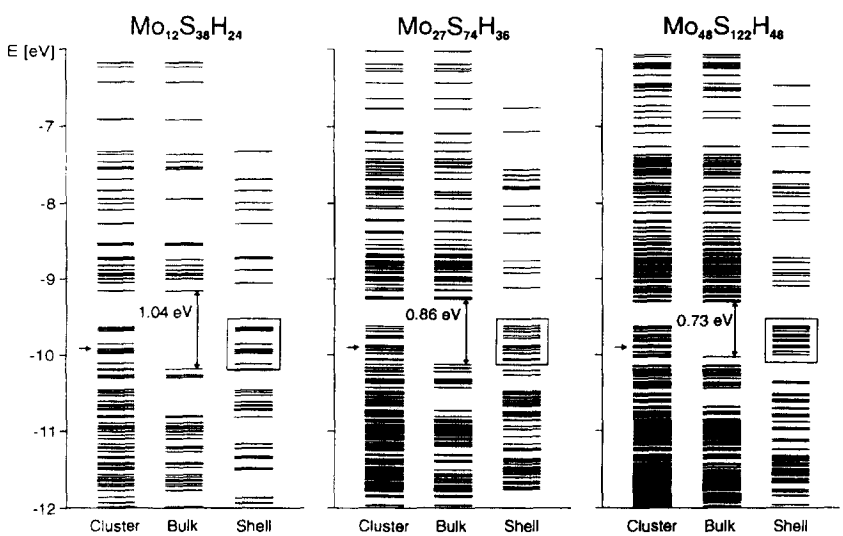


Fig. 2. Comparison of the $Mo_{12}S_{38}H_{24}$, $Mo_{27}S_{74}H_{36}$ and $Mo_{48}S_{122}H_{48}$ cluster energy levels from $-12$ to $-6$ eV before and after projecting out the bulk- and the shell-localized states. The HOMO is marked with an arrow, the band gap of the bulk is indicated and the shell-localized states falling into this band gap are framed.

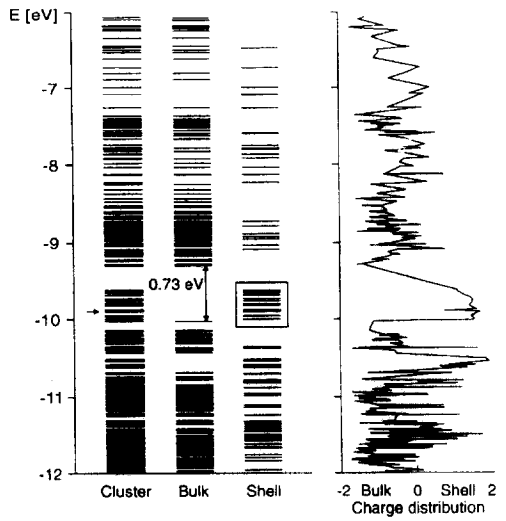


Fig. 3. Left: Part of the $Mo_{48}S_{122}H_{48}$ cluster energy levels before and after separation of the bulk- and the shell-localized states. The HOMO is marked with an arrow, the band gap of the bulk is indicated and the shell-localized states falling into this band gap are framed. Right: $\Delta Q_i$ according to Eq. (5) for each energy level $i$. The values are connected with a straight line.

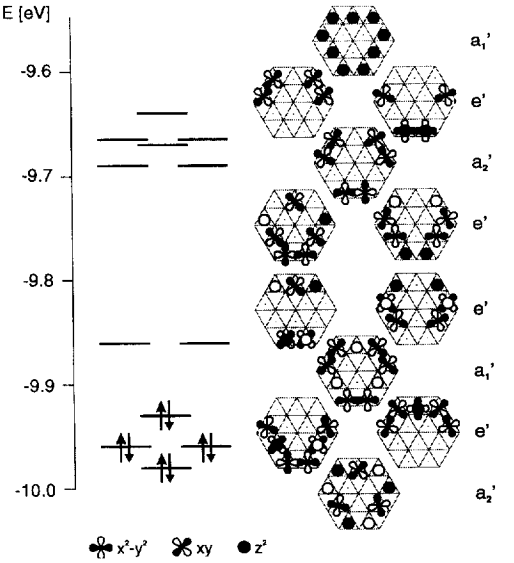


Scheme 4. Surface state Mo(4d) orbitals of the $Mo_{12}S_{38}H_{24}$ cluster.

HOMO/LUMO region to the shell, shaded in Scheme 2, is straightforward. This means that the surface states, the nature of which we will analyze below, can be attributed to the shell Mo and S atoms. The assignment of the one-electron energy levels to bulk- and to shell-localized states leads to the cluster/bulk/shell bar diagram on the left side of Fig. 3. The previously missed energy gap is present in the bulk. Fig. 2 has been constructed in the same way. The band gap of the bulk decreases with increasing cluster size and it finally reaches the limiting $^2_\infty[MoS_2]$ value as reported in Table 3. The bulk can be named as Brus part of the cluster because the development of the band gap fits into the quantum-size picture. We note that the energy of the HOMO changes only little with increasing cluster size. It lies above the HOMO of the bulk. We therefore conclude that the surface of the considered clusters is paramagnetic while the bulk is diamagnetic.

The surface states falling into the band gap of the clusters are framed in Figs. 2 and 3. They can be identified as $4d_{x^2-y^2}$, $4d_{xy}$, and $4d_{z^2}$ orbitals of the shell Mo atoms with some S(3p) contributions. This is illustrated in the simplified Scheme 4 for $Mo_{12}S_{38}H_{24}$ which carries four single and four double degenerate Mo(4d) type levels within the band gap. In the bulk of the clusters and in the infinite $^2_\infty[MoS_2]$ slab the Mo($4d_{x^2-y^2}$, $4d_{xy}$, $4d_{z^2}$) orbitals are split to the valence and to the conduction band. This means that the shell Mo atoms of the cluster

Table 3
Energy gap between the highest occupied and the lowest unoccupied bulk states; in the last column the HOMO (clusters) or the Fermi level (monolayer) are listed

| Cluster | Energy gap (eV) | | | HOMO or Fermi level (eV) |
|---|---|---|---|---|
| | lower limit | upper limit | gap width | |
| $Mo_{12}S_{38}H_{24}$ | −10.2 | −9.16 | 1.04 | −9.93 |
| $Mo_{27}S_{74}H_{36}$ | −10.13 | −9.27 | 0.86 | −9.9 |
| $Mo_{48}S_{122}H_{48}$ | −10.03 | −9.31 | 0.73 | −9.9 |
| monolayer | −9.87 | −9.4 | 0.47 | −9.87 |

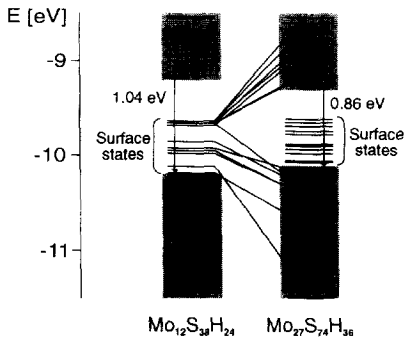


Fig. 4. Correlation diagram of the 12 surface Mo(4d) states localized at the 9 shell Mo atoms of the $Mo_{12}S_{38}H_{24}$ cluster shown in Scheme 4 and of the corresponding states in the larger $Mo_{27}S_{74}H_{36}$ cluster where the same 9 atoms now belong to the bulk. Also shown is the stabilization of the three $S(3p_x,3p_y)$ type surface states by coordination with the added molybdenum atoms.

"feel" a weaker field than the bulk ones. All of them are sixfold coordinated by sulphur, however. In addition to the 12 Mo(4d) type levels three sulphur localized states, $a_2''$ and e'', are present, less than one tenth of an eV above the HOMO of the bulk. They originate from antibonding interactions of $S(3p_x,3p_y)$ type orbitals of the upper and lower slabs of surface sulphur atoms with some Mo(4d) mixing in. To keep Scheme 4 as simple and general as possible they are not shown. The reason why the surface states disappear in the infinite slab can be understood from the correlation diagram in Fig. 4 which illustrates how the 12 surface Mo(4d) states of the $Mo_{12}S_{38}H_{24}$ cluster transfer to bulk states in the larger $Mo_{27}S_{74}H_{36}$ cluster. We see which Mo(4d) type orbitals shift upwards and downwards due to antibonding and bonding interactions with the 4d orbitals of the added 15 Mo atoms which form themselves the surface states in the larger cluster. The Mo–Mo distances of 3.16 Å allow sufficient overlap to cause this splitting. The surface states belonging to the $S(3p_x,3p_y)$ type orbitals are stabilized by the new Mo atom shell and shift deep into the valence band.

The ratio of shell Mo atoms to bulk Mo atoms $SC_n$ for the $D_{3h} - (MoS_2)_{3n^2}S_2(H_2S)_{6n}$, $n = 1,2,\cdots$ clusters is

$$SC_n = \frac{2n-1}{n^2-2n+1}, \qquad (6)$$

which becomes equal to $2/n$ for large $n$. This means that for example a cluster of 30000 Mo atoms contains about 600 Mo atoms which act as surface states. We can imagine that there are instances where the bulk states act to some extent independently of the shell, depending on the strength of coupling between the bulk and the shell atoms involved. In luminescence experiments the surface states may act like quencher molecules, and competition between thermal and radiative decay is expected to depend on the cluster size.

This is the place to add some observations concerning the charges of the shell atoms, which are of importance in the context of chemical reactivity. The charges of the shell sulphur atoms show a strong dependence on the coordination to Mo. The corner S atoms of $Mo_{48}S_{122}H_{48}$ are charged by $-0.30$, and the other S atoms coordinated to only one Mo are charged by $-0.36$. The bridging surface S, coordinated to two Mo, are positively charged by $+0.30$, however. The corner Mo atoms are charged quite strongly, by $+0.71$. The other surface shell Mo atoms carry a charge of $+0.19$ up to $+0.40$, depending on the exact location. The charges of the bulk Mo and S atoms are more homogeneous. The Mo and S of the inmost core shell of $Mo_{48}S_{122}H_{48}$ are charged by $+0.16$ and $-0.08$, respectively. The smaller clusters show similar features. This is to be compared with the charges obtained for the infinite layer $^2_\infty[MoS_2]$ which are $+0.30$ and $-0.15$ on Mo and S, respectively.

We now come to the link between the MO cluster calculations and the CO treatment of stacked clus-

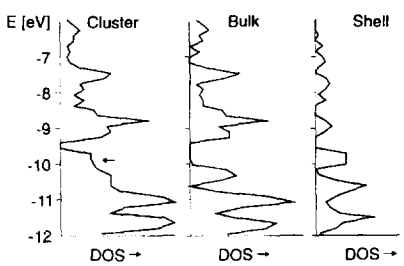


Fig. 5. $Mo_{48}S_{122}H_{48}$ cluster density of states (DOS) of the whole cluster and projection of the bulk and the shell contributions in the range of $-12$ to $-6$ eV. The Fermi level is indicated with an arrow. An energy gap opens up around the Fermi energy in the bulk-localized DOS.

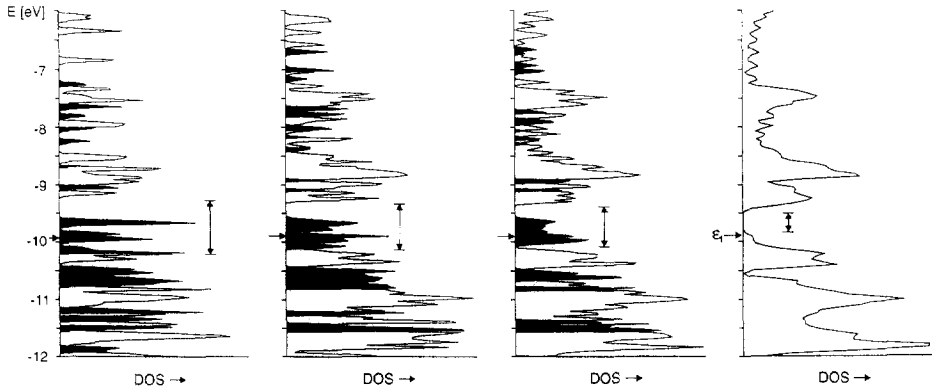


Fig. 6. Densities of states (DOS) between −12 and −6 eV in the Fermi level region of the cluster chains $^{1}_{\infty}[Mo_{12}S_{38}H_{24}]$, $^{1}_{\infty}[Mo_{27}S_{74}H_{36}]$, $^{1}_{\infty}[Mo_{48}S_{122}H_{48}]$, and the infinite layer $^{2}_{\infty}[MoS_2]$, from left to right. For a projection of the S(3s), S(3p), and the Mo(4d) contributions to the total DOS of $^{2}_{\infty}[MoS_2]$ we refer to Fig. 1. The contributions of the shell of the chains are shaded and the energy gap of the bulk is indicated. The surface states falling into the band gap of the clusters and the narrowing of the bulk-localized energy gap with increasing cluster size are distinct.

ters. Instead of drawing the energy levels resulting from MO calculations as bars we can draw them as number of energy levels per energy interval. This is the equivalent to the DOS plot in CO computations. The larger the cluster, the smoother the plot will appear. A MO-DOS plot without smoothing is shown in Fig. 5 for the $Mo_{48}S_{122}H_{48}$ cluster. The information in this plot is the same as in the bar diagram of Fig. 3. Inspection of the different contributions shows that the energy levels are distinguished into a region between −20.9 and −19.8 eV consisting of S(3s) mainly and a S–H bonding region between −14.4 and −13.9 eV, which are not shown. Then we find the S(3p) contributions between −12.7 and −10.0 eV overlapping slightly with the Mo(4d) region between −10.4 and −6.0 eV, where the HOMO (or Fermi level) at −9.9 eV is falling into. The S–H antibonding levels and Mo(5s) and Mo(5p) contributions stretch out above −1.0 eV. The LUMO is nearly degenerate with the HOMO in the cluster and the surface states can be projected out as already discussed. The strong surface localization of the levels around the HOMO can readily be recognized.

This partitioning can also be nicely illustrated in the infinite cluster chain where the shell atoms lie on the periphery of an infinite tube. The information is the same as before. In Fig. 6 we show from left to right the DOS plots of $^{1}_{\infty}[Mo_{12}S_{38}H_{24}]$, $^{1}_{\infty}[Mo_{27}S_{74}H_{36}]$, $^{1}_{\infty}[Mo_{48}S_{122}H_{48}]$, and $^{2}_{\infty}[MoS_2]$. The Fermi energy is marked with an arrow in each case and the shell-localized states are projected out as described in the computational section. They are shaded and can therefore be distinguished from the bulk-localized states. For the clusters we find, as before, that in the region of the Fermi level surface states fill up the band gap. The band gap of the bulk calculated for the different cluster chains is the same as that for the isolated clusters, as expected since the distances between the individual clusters is 10 Å, and the aim of this figure is to illustrate the close link between CO and MO results.

## 4. Conclusions

EHMO calculations on clusters of respectable size have become relatively easy and inexpensive. Because of the large number of states of such particles interpretational tools to decompose surface states from the bulk states are needed. Such tools are expected to be helpful to advance the understanding of nanometer-sized particles, which have gained increasing interest recently. In this report we describe a projection procedure as an instrument to separately analyze the electronic states of surface and bulk regions. It allows to discuss surface states in terms of specific atoms, coordination numbers, oxidation states, and connectivities and it gives new insight

into the size quantization of clusters. The procedure is general and can be used for studying systems of different composition, different structure and different size up to a few hundred or thousand atoms. Since layered compounds with equivalent top and bottom surface atoms are easier to be described than other structures, because only the periphery atoms have to be considered apart, we have chosen $D_{3h}-(MoS_2)_{3n^2}S_2(H_2S)_{6n}$, $n = 1,2,\cdots$ clusters as an illustrative and interesting example. We show that these clusters can be divided into a bulk region, bearing the expected quantum-size behaviour, and a shell, responsible for the surface states originating from the outermost molybdenum atoms and being of mainly $4d_{x^2-y^2}$, $4d_{xy}$, and $4d_{z^2}$ type with some S(3p) contributions. These surface states are also present in an ideal but real $MoS_2$ crystal and one can estimate their number from our calculations.

## Acknowledgements

We acknowledge financial support by the Schweizerische Nationalfonds zur Förderung der wissenschaftlichen Forschung grant No. 20-40598.94/1 and by the Swiss Federal Office of Energy BEW grant No. (93)034.

## References

[1] I. Tamm, Physik. Z. Sowjetunion 1 (1932) 733; Z. Physik 76 (1932) 849.
[2] E.T. Goodwin, Proc. Cambridge Phil. Soc. 35 (1939) 221, 232.
[3] W. Shockley, Phys. Rev. 56 (1939) 317.
[4] J. Koutecký, Phys. Rev. 108 (1957) 13.
[5] R. Hoffmann, Solids and surfaces: a chemist's view of bonding in extended structures (VCH, New York, 1988).
[6] Wo. Ostwald, Die Welt der vernachlässigten Dimensionen (Verlag Theodor von Steinkopff, Dresden und Leipzig, 1921).
[7] Y. Wang and N. Herron, J. Phys. Chem. 95 (1991) 525.
[8] L.E. Brus, J. Chem. Phys. 79 (1983) 5566; J. Phys. Chem. 90 (1986) 2555.
[9] T. Rajh, M.W. Peterson, J.A Turner and A. Nozik, J. Electroanal. Chem. 228 (1987) 55.
[10] Y. Nosaka, J. Phys. Chem. 95 (1991) 5054.
[11] R.P. Messmer and G.D. Watkins, Radiat. Effects 9 (1971) 9.
[12] R. Hoffmann, Rev. Mod. Phys. 60 (1988) 601.
[13] R.A. Wheeler, L. Piela and R. Hoffmann, J. Am. Chem. Soc. 110 (1988) 7302.
[14] G. Calzaferri and M. Brändle, ICONC&INPUTC, Quantum Chemistry Program Exchange, QCPE Program QCMP No. 116, QCPE Bull. 12 (1992) 73, update May 1993.
[15] C.F. Zinola, A.J. Arvia, G.L. Estiu and E.A. Castro, J. Phys. Chem. 98 (1994) 7566.
[16] J.A. Wilson and A.D. Yoffe, Advan. Phys. 18 (1969) 193.
[17] M. Kertesz and R. Hoffmann, J. Am. Chem. Soc. 106 (1984) 3453.
[18] H. Tributsch, Phys. Chem. Mater. Low-Dimensional Struct. 14 (1992) 83.
[19] K.K. Kam and B.A. Parkinson, J. Phys. Chem. 86 (1982) 463.
[20] C. Rong and X. Qin, J. Mol. Catal. 64 (1991) 321.
[21] E. Sandré, R. Brec and J. Rouxel, J. Solid State Chem. 88 (1990) 269.
[22] M.W. Peterson, M.T. Nenadovic, T. Rajh, R. Herak, O.I. Micic, J.P. Goral and A.J. Nozik, J. Phys. Chem. 92 (1988) 1400.
[23] A.B. Anderson, Z.Y. Al-Saigh and W.K. Hall, J. Phys. Chem. 92 (1988) 803.
[24] M. Brändle, G. Calzaferri and M. Lanz, Chimia 48 (1994) 293.
[25] R.G. Dickinson and L. Pauling, J. Am. Chem. Soc. 45 (1923) 1466.
[26] R. Hoffmann, J. Chem. Phys. 39 (1963) 1397.
[27] M.C. Zonnevylle and R. Hoffmann, Surface Sci. 199 (1988) 320.
[28] E. Clementi and C. Roetti, At. Data Nucl. Data Tables 14 (1974) 439.
[29] M. Brändle and G. Calzaferri, Helv. Chim. Acta 76 (1993) 924.
[30] M. Wolfsberg and L. Helmholz, J. Chem. Phys. 20 (1952) 837.
[31] J.H. Ammeter, H.-B. Bürgi, J.C. Thibeault and R. Hoffmann, J. Am. Chem. Soc. 100 (1978) 3686.
[32] G. Calzaferri, L. Forss and I. Kamber, J. Phys. Chem. 93 (1989) 5366; G. Calzaferri and C. Marcolli, J. Phys. Chem. 99 (1995) 3895.
[33] V.I. Baranovskii and A.B. Nikol'skii, Teor. Eksp. Khim. 3 (1967) 527.
[34] H. Basch, A. Viste and H.B. Gray, Theoret. Chim. Acta 3 (1965) 458.
[35] L. Libit and R. Hoffmann, J. Am. Chem. Soc. 96 (1974) 1370.
[36] R.S. Mulliken, J. Chem. Phys. 23 (1955) 1833, 1841, 2338, 2343.
[37] M.-H. Whangbo and R. Hoffmann, J. Am. Chem. Soc. 100 (1978) 6093.
[38] M.-H. Whangbo, M. Evain, T. Hughbanks, M. Kertesz, S. Wijeysekera, C. Wilker, C. Zheng and R. Hoffmann, EHMACC Extended Hückel Molecular, Crystal and Properties Package, Quantum Chemistry Program Exchange, QCPE Program QCPE No. 571, QCPE Bull. 9 (1989).
[39] M. Brändle and G. Calzaferri, Helv. Chim. Acta 76 (1993) 2350.
[40] R. Coehoorn, C. Haas, J. Dijkstra, C.J.F. Flipse, R.A. de Groot and A. Wold, Phys. Rev. B 35 (1987) 6195;
[41] F.R. Shepherd and P.M. Williams, J. Phys. C 7 (1974) 4427.
[42] J.C. McMenamin and W.E. Spicer, Phys. Rev. Letters 29 (1972) 1501.